The Astronomical Journal, 140:1672–1686, 2010 December doi:10.1088/0004-6256/140/6/1672

FIDUCIAL STELLAR POPULATION SEQUENCES FOR THE VJK_S PHOTOMETRIC SYSTEM

Crystal M. Brasseur[1], Peter B. Stetson[2], Don A. VandenBerg[1],
Luca Casagrande[3], Giuseppe Bono[4], and Massimo Dall'Ora[5]
[1] Department of Physics and Astronomy, University of Victoria, P.O. Box 3055, Victoria, BC, V8W 3P6, Canada; brasseur@uvic.ca, vandenbe@uvic.ca
[2] Herzberg Institute of Astrophysics, National Research Council Canada, 5071 W. Saanich Rd., Victoria, BC, V9E 2E7, Canada; peter.stetson@nrc-cnrc.gc.ca
[3] Max-Planck-Institut für Astrophysik, Postfach 1317, 85748 Garching, Germany; lcasagrande@mpa-garching.mpg.de
[4] Università di Roma Tor Vergata, Via della Ricerca Scientifica 1, 00133 Rome, Italy; giuseppe.bono@oa-roma.inaf.it
[5] INAF-Osservatorio Astronomico di Capodimonte, Via Moiariello 16, 80131 Napoli, Italy; dallora@na.astro.it
Received 2010 June 26; accepted 2010 September 15; published 2010 October 26

ABSTRACT

We have obtained broadband near-infrared photometry for seven Galactic star clusters (M 92, M 15, M 13, M 5, NGC 1851, M 71, and NGC 6791) using the WIRCam wide-field imager on the Canada–France–Hawaii Telescope, supplemented by images of NGC 1851 taken with HAWK-I on the Very Large Telescope. In addition, Two Micron All Sky Survey (2MASS) observations of the [Fe/H] $\approx$ 0.0 open cluster M 67 were added to the cluster database. From the resultant $(V - J) - V$ and $(V - K_S) - V$ color–magnitude diagrams (CMDs), fiducial sequences spanning the range in metallicity, $-2.4 \lesssim$ [Fe/H] $\lesssim +0.3$, have been defined which extend (for most clusters) from the tip of the red giant branch (RGB) to ~2.5 mag below the main-sequence turnoff. These fiducials provide a valuable set of empirical isochrones for the interpretation of stellar population data in the 2MASS system. We also compare our newly derived CMDs to Victoria isochrones that have been transformed to the observed plane using recent empirical and theoretical color–$T_{\rm eff}$ relations. The models are able to reproduce the entire CMDs of clusters more metal rich than [Fe/H] ≈ -1.4 quite well, on the assumption of the same reddenings and distance moduli that yield good fits of the same isochrones to Johnson–Cousins $BV(RI)_C$ photometry. However, the predicted giant branches become systematically redder than the observed RGBs as the cluster metallicity decreases. Possible explanations for these discrepancies are discussed.

Key words: globular clusters: general – globular clusters: individual (M5, M13, M15, M92, NGC1851, 47 Tucanae) – Hertzsprung–Russell and C–M diagrams – open clusters and associations: general – open clusters and associations: individual (M67, NGC6791) – stars: fundamental parameters – stars: general

1. INTRODUCTION

The Two Micron All Sky Survey (2MASS) has uniformly scanned the entire sky in three near-infrared bands, JHK_S. Cataloging more than 300 million point sources, 2MASS observations are not only advancing our understanding of stars, but they also provide the photometric standards used to calibrate all other JHK_S photometry. In recent years, a new generation of JHK_S-equipped observing facilities have come online, driven by the benefits of observing at these longer wavelengths. In particular, reduced dust attenuation allows the near-infrared to be a better probe of stellar populations in dust-obscured and heavily reddened galaxies. Furthermore, the integrated luminosities of intermediate-age and old stellar populations, which are predominantly due to their asymptotic giant branch (AGB) and red giant branch (RGB) stars, are brightest at these longer wavelengths.

As the infrared (IR) region of the electromagnetic spectrum receives growing attention in modern astrophysics, it becomes desirable to have deep near-IR photometry for Galactic star clusters. Currently, the available near-IR fiducials of these systems remain restricted in both metallicity and luminosity, with the observations rarely extending to fainter magnitudes than the base of the RGB (e.g., Frogel et al. 1983; Valenti et al. 2007; Ferraro et al. 2000). Star clusters are the ideal stellar populations to observe because, notwithstanding a growing number of exceptions (e.g., ω Cen), their stars are or can be considered homogeneous in both age and initial chemical composition to a rather good approximation, at least for a number of purposes. Therefore, observations of these systems provide us with exceedingly valuable stellar population templates across a broad range of stellar parameter space, as well as the data which are needed to test and refine the predicted colors from model atmospheres and the temperatures given by stellar evolutionary models.

Stellar population studies rely on the accuracy of both color–$T_{\rm eff}$ relations and the stellar $T_{\rm eff}$ scale in order to derive the ages, metallicities, and star formation histories of stellar systems based on isochrone fits to observed color–magnitude diagrams (CMDs). One way to test these relations is to obtain photometry in many bandpasses and then to determine the level of consistency across all possible CMDs (and color–color diagrams) that can be generated. While considerable work has been carried out to test and improve the color transformations for the $BV(RI)_C$ and Strömgren filter systems (e.g., VandenBerg & Clem 2003; Clem et al. 2004), very little has been done to date on the color–$T_{\rm eff}$ relations for the near-IR (two of the few works to date are Pinsonneault et al. 2004 and Grocholski & Sarajedini 2003).

In this paper, new CMDs for open and globular star clusters, along with published data for field subdwarfs, are compared with isochrones in order to assess the reliability of recent $(V-J)$–$T_{\rm eff}$ and $(V - K_S)$–$T_{\rm eff}$ relations. Additionally, and perhaps most importantly, we can for the first time evaluate the consistency of the isochrone fits across optical and infrared colors. The companion work to this paper, VandenBerg et al. (2010); hereafter known as VCS10), focuses on the color–$T_{\rm eff}$ relations for the Johnson–Cousins $BV(RI)_C$ photometric system. In both papers, two recently developed sets of color transformations are tested. The first of these has been derived (see VCS10) from

Table 1
Description of Observations for Each Target

Cluster	Dates of Observations	Exposure time in J	Exposure time in K	Weather Conditions
M 15	2008 Aug 10–18	45 s × 40, 5 s × 7	20 s × 97	Photometric
M 92	2008 Aug 10–18	25 s × 5, 45 s × 14, 5 s × 21	20 s × 127, 5 s × 19	Photometric
M 13	2008 Aug 11 and 12	45 s × 25	20 s × 153	Photometric
M 5	2009 Jun 11	20 s × 56	...	Photometric
NGC 1851	2008 Jan 30	...	10 s × 139	Photometric
M 71	2008 Aug 10–18	5 s × 22	5 s × 45	Photometric
NGC 6791	2008 Aug 10–18	5 s × 21	...	Photometric

the latest MARCS model atmospheres (Gustafsson et al. 2008), while the second is the set of empirical relations developed by Casagrande et al. (2010) who used the infrared flux method (IRFM) to produce color–$T_{\rm eff}$ relations for dwarf and subgiant stars spanning a large range in metallicity.

Addressing the need for precise fiducial sequences in the near-infrared, we have obtained observations of the seven Galactic star clusters, M 92, M 15, M 13, M 5, NGC 1851, M 71 and NGC 6791. In Section 2, we describe our observing programs and present salient details concerning the reduction of the data—including, in particular, the calibration of our photometry to the standard 2MASS system. In Section 2.1, the CMDs and cluster fiducials are presented which provide template stellar population sequences for the range in metallicity, $-2.4 \lesssim$ [Fe/H] $\lesssim +0.3$. An examination of how well isochrones that employ the synthetic MARCS, and the empirical Casagrande et al. (2010), color–$T_{\rm eff}$ relations are able to reproduce the observed VJK_S photometry of the local subdwarfs and of our target clusters is presented in Section 3. Finally, a short summary of our results, as well as a brief discussion of the usefulness of the derived fiducial sequences for stellar populations research, is given in Section 4.

2. OBSERVATIONS

In the 2008B semester, we received WIRCam time on the Canada–France–Hawaii Telescope (CFHT) to observe five Galactic star clusters (NGC 6791, M 13, M 15, M 92 and M 71) in J and K_S. In the following semester (2009A), we obtained observations of M 5, but only in the J band due to poor weather conditions. In addition, K_S-band images of NGC 1851 that had been previously collected by two of us (G.B. and M.D.) using the Very Large Telescope (VLT) HAWK-I detector were included in the data set. All of our CFHT observations aimed to reach a signal-to-noise ratio of 25 at ∼2.5 mag below the main-sequence turnoff (MSTO) of each cluster. To accomplish this, a series of long exposures, together with several short-exposure images (which were critical for the calibration of our fields to 2MASS photometry), were taken in the J and K_S filters for each cluster on our target list. By taking a series of exposures, each star was detected multiple times, thereby helping to improve the precision of the final photometry. We direct the reader to Table 1 which lists the image properties of each cluster. Unlike optical photometry, where one would separately observe standard star fields, the 2MASS All-Sky Point Source Catalog contains enough stars in each of our clusters which can be used as standards. For example, M 13 has 3221 stars in the 2MASS All-Sky Point Source Catalog within 30 arcmin of its center. Of these, we selected stars with the lowest claimed photometric errors (typically errors < 0.02) for the calibration of our frames.

In addition to the on-target images, it was necessary to obtain a large number of off-target images of the sky because both the spatial and temporal variations of atmospheric emission in the IR are quite considerable (∼10% over a timespan of as little as 10 minutes). Indeed, particular care was taken in determining how to construct and subtract a sky image from a target image, since the quality of a processed image is dominated by precisely how this subtraction is carried out. In order to minimize the effects of the variable sky on our photometry, we decided to image an equal number of sky frames off-target as science frames on-target. We also chose to employ a large dither pattern so as to remove bad pixels when median combining the frames. Once observed, images were pre-processed by CFHT staff using the WIRCam pipeline. This included flat fielding, bias and dark subtraction, as well as sky subtraction.

Upon receiving the pre-processed images, instrumental magnitudes for all stars were obtained using the point-spread function (PSF) modeling and fitting techniques in the DAOPHOT/ALLSTAR/ALLFRAME packages (Stetson 1987; Stetson & Harris 1988). In essence, these programs work by detecting stars on a specific image, building a model PSF from a few isolated, bright stars and then subtracting this PSF from all stars detected. (For a more detailed description of how how these programs work, see Stetson 1987.) The standard star calibration directly to 2MASS stars in the same frame, was done by solving for the zero point, and color terms which accounts for the difference in the central wavelengths of the CFHT and 2MASS J and K filters.

One can check the overall quality of our transformed magnitudes by comparing stars in common between our fields and the 2MASS catalog. Two examples of such comparisons are shown in Figures 1 and 2, for NGC 1851 and M 92, where the differences between the standard 2MASS magnitudes and our final calibrated ones are plotted against both magnitude and color. Reassuringly, the horizontal lines corresponding to zero difference appear to pass through the densest concentration of points in all plots. Moreover, there seem to be no strong systematic trends as a function of color that would indicate the need for higher order color terms in the photometric solutions.

To produce the CMDs, our final photometry for each cluster was combined with V-band data (see Stetson 2000; Stetson 2005). Our CMD of NGC 1851, which is from VLT observations, extends from near the RGB tip to ∼3 mag below the MSTO. For the remaining six clusters, which were observed using the CFHT, we were able to obtain observations only for magnitudes fainter than the base of the RGB. The upper giant-branch stars were saturated in all of our frames, despite observing the target clusters with the shortest exposures possible on WIRCam, This problem occurred mainly because the seeing was 0.″3 to 0.″5 better than we had requested during the nights of observation, which resulted in a more concentrated PSF.

Thus, in order to populate the RGBs of the clusters that were observed using the CFHT, we queried the 2MASS catalog for

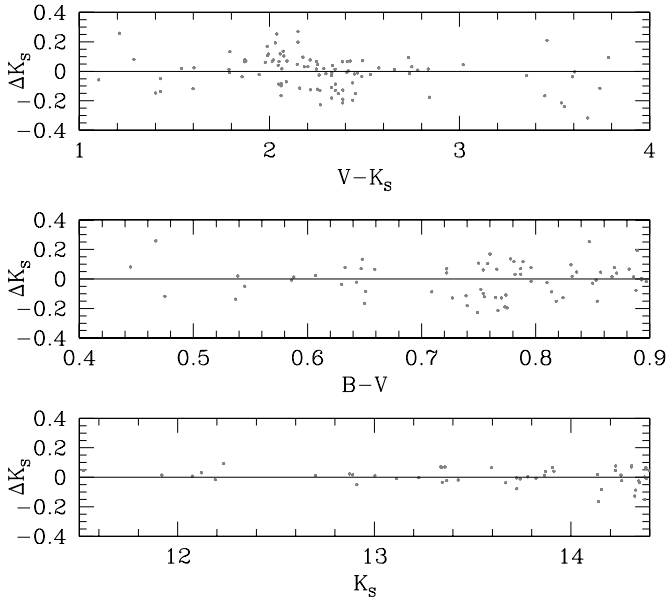

Figure 1. K_S-band photometric differences for stars observed in both 2MASS and our VLT fields for NGC 1851.

all of the stars within 30′ of the center of each cluster. With a photometric sensitivity of 10 sigma at $J = 15.8$ and $K_S = 14.3$ mag, 2MASS observations extend at least to the base of the giant branch for each of our target clusters. The 2MASS photometry for the selected giant-branch stars in each system (Skrutskie et al. 2006) was then combined with *V*-band photometry for the same stars (Stetson 2000, 2005).

Although it is ideal to have homogeneous observations for the entire range in cluster magnitude, the zero points of our WIRCam photometry were set using 2MASS observations from the same catalog that was used to identify the RGB stars. Therefore, in principle, one should expect that there are no differences between these observations. However, in practice, the possibility that uncertainties in the zero points may be appreciable should be kept in mind when employing the resultant CMDs and fiducial sequences. A list of our observed clusters and our adopted reddening and distance moduli are given in Table 2.

Table 2
Properties of the Galactic Star Clusters in Our Survey

Cluster	Type	α	δ	[Fe/H]	$(m-M)_V$	$E(B-V)$
M 15	Globular	21:29:58	+12:10:01	−2.4	15.29	0.108
M 92	Globular	17:17:07	+43:08:12	−2.4	14.62	0.023
M 13	Globular	16:41:41	+36:27:37	−1.60	14.40	0.016
M 5	Globular	15:18:36	+02:05:00	−1.40	14.45	0.038
NGC 1851	Globular	05:14:06	−40:02:50	−1.40	15.50	0.034
M 71	Globular	19:53:46	+18:46:42	−0.80	13.78	0.220
NGC 6791	Open	19:20:53	+37:46:30	+0.3	13.57	0.150

2.1. Fiducials

Fiducial sequences are ridge lines of the stellar loci in color–magnitude space. The definition of these fiducials from cluster photometry is often based on visual inspection of the CMD, since automated scripts typically give poor results in regions of low star counts and where the magnitude varies weakly with color, such as the subgiant branch (SGB). Moreover, contamination from field, AGB, binary, and horizontal-branch (HB) stars can significantly skew the computed locus. For these reasons, we have derived all fiducials by dividing the magnitude axis into small bins (typically ∼0.15 mag wide, or smaller in regions of nearly constant magnitude) and then calculating the median color of those stars which we judge to belong to the cluster.

We present our observed CMDs in Figures 3–9 with 2MASS, CFHT/WIRCam, and VLT/HAWK-I photometry plotted as open circles, filled circles, and open triangles, respectively. Overlaid on the CMDs are the derived fiducial sequences spanning the MS, SGB, and RGB (see Tables 2–9). In the case of M 13, M 92, and M 15, there were insufficient points to define the fiducial for the SGB; consequently, the latest Victoria–Regina Models by D. A. VandenBerg et al. (2010, in preparation) of the same metallicity of each cluster were used to define the transition from the MS to the lower RGB in these cases (such points are marked with an asterisk in the tables).

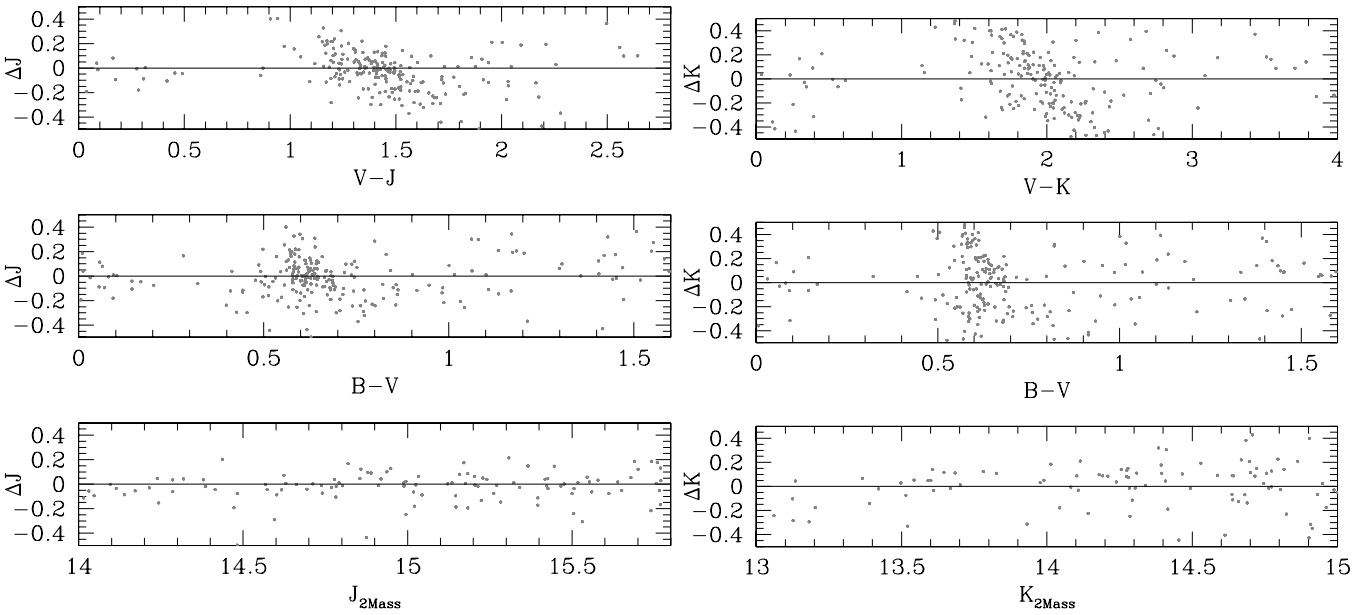

Figure 2. *J*- and K_S-band photometric differences for stars observed in both 2MASS and our CFHT fields for M 92.

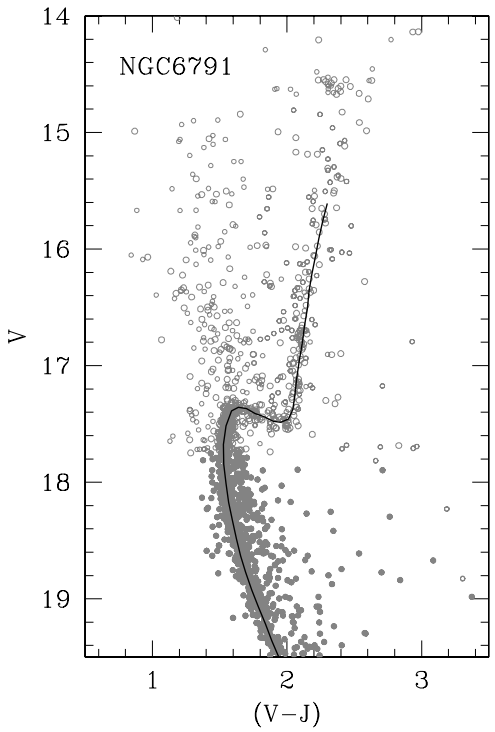

Figure 3. Derived $V-(V-J)$ fiducial sequence of NGC 6791 overlaying CFHT (filled circles) and 2MASS (open circles) photometry.

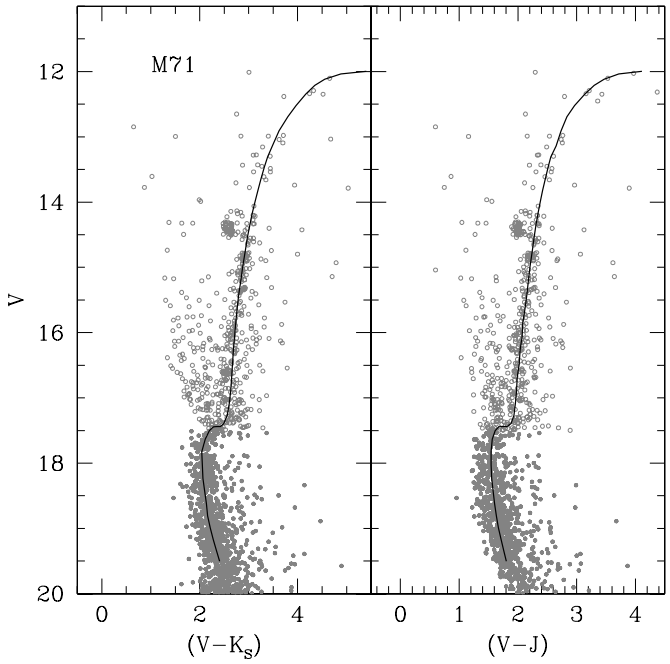

Figure 4. Derived $V-(V-K_S)$ and $V-(V-J)$ fiducial sequences of M 71 overlaying CFHT (filled circles) and 2MASS (open circles) photometry.

3. TESTING THE COLOR–$T_{\rm eff}$ RELATIONS USING OBSERVATIONS OF FIELD SUBDWARFS AND STAR CLUSTERS

Transforming isochrones from the theoretical $\log T_{\rm eff}$–$M_{\rm bol}$ plane to an observed CMD is accomplished through the use of color–$T_{\rm eff}$ relations to link the fundamental stellar parameters to photometric indices. In this section, we investigate two recently developed color transformations. The first of these is an empirical relation developed by (Casagrande et al. 2010; hereafter referred to as CRMBA), who have applied the IRFM to a large sample of dwarf and subgiant stars of varying metallicity. They present their results as a set of polynomials which relate many photometric indices to $T_{\rm eff}$ and [Fe/H]. This empirical color–$T_{\rm eff}$ relation has the advantage of being largely model independent, but it has the limitation of being applicable only to dwarf and SGB stars.

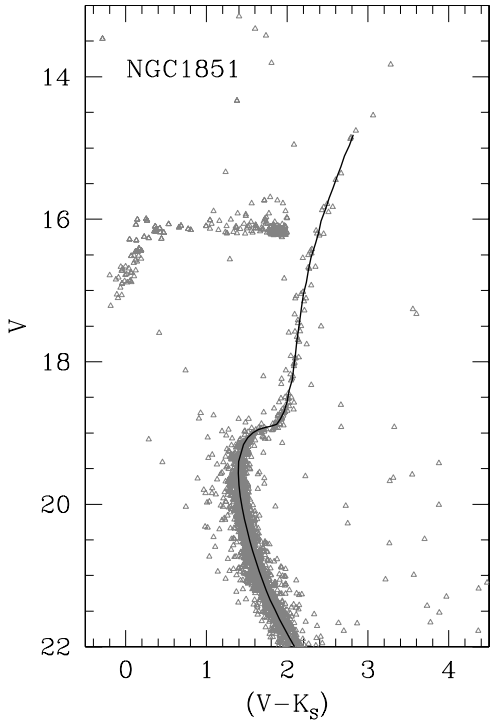

Figure 5. Derived $V-(V-K_S)$ fiducial sequence of NGC 1851 overlaying HAWK-I K_S photometry.

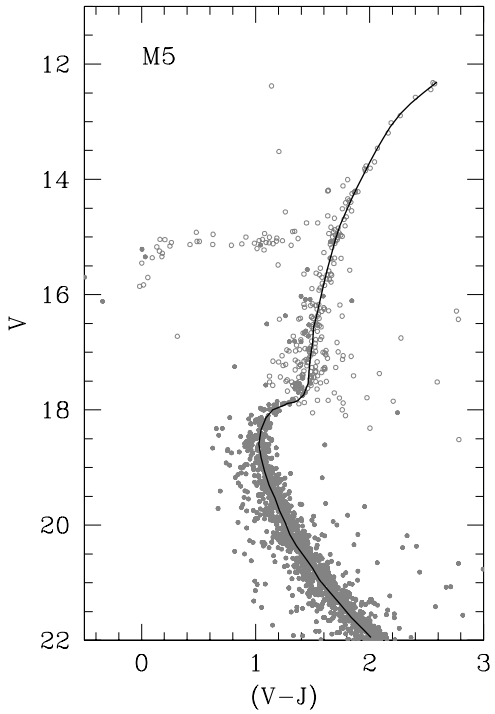

Figure 6. Derived $V-(V-J)$ fiducial sequence of M 5 overlaying CFHT (filled circles) and 2MASS (open circles) photometry.

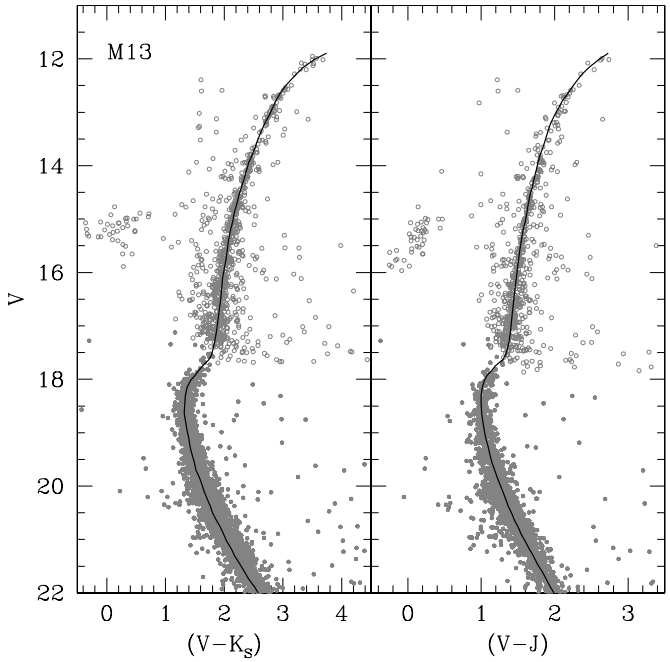

Figure 7. Derived $V-(V-K_S)$ and $V-(V-J)$ fiducial sequences of M 13 overlaying CFHT (filled circles) and 2MASS (open circles) photometry.

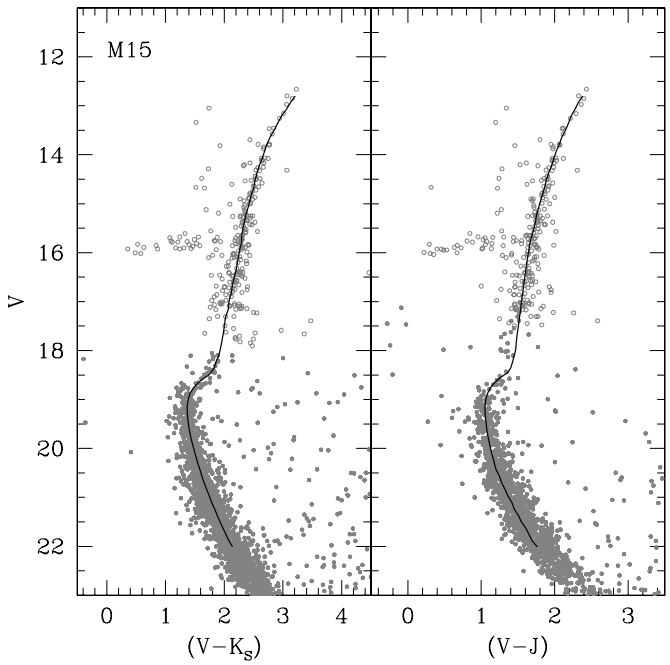

Figure 8. Derived $V-(V-K_S)$ and $V-(V-J)$ fiducial sequences of M 15 overlaying CFHT (filled circles) and 2MASS (open circles) photometry.

The second relation was derived by one of us (L.C.) from synthetic spectra based on the latest MARCS model atmospheres (Gustafsson et al. 2008) using the procedures described in VCS10, with the 2MASS filter transmission curves, absolute calibration and zero points reported in Casagrande et al. (2006). The MARCS models consist of plane–parallel (for dwarf and SGB stars) and spherical (for giant stars) line-blanketed, flux-constant stellar atmospheres for large ranges in effective temperature, surface gravity, and chemical composition. By convolving the spectra derived from these atmospheres with the appropriate filter transmission functions, large tables were produced that

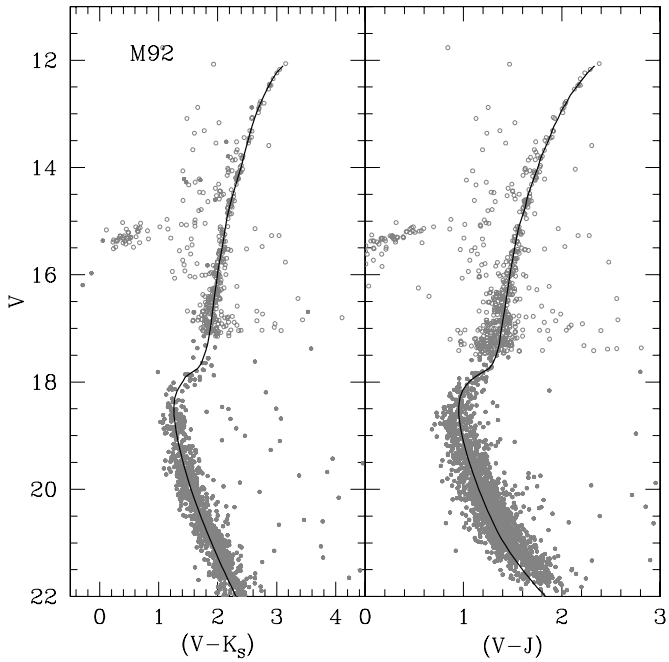

Figure 9. Derived $V-(V-K_S)$ and $V-(V-J)$ fiducial sequences of M 92 overlaying CFHT (filled circles) and 2MASS (open circles) photometry.

provide the synthetic magnitudes as functions of [Fe/H], $T_{\rm eff}$, and $\log g$. Theoretical relations such as these have the advantage over the CRMBA relation that the desired photometric indices for any given star or stellar model can be obtained simply by interpolating it in the grid of synthetic colors for its [Fe/H], $\log g$, and $T_{\rm eff}$ values. However, their accuracy relies heavily on whether or not the synthetic spectra are able to reproduce the observed spectra of stars, and on how well the filter transmission functions and zero points are defined. It should also be noted that we apply the slight modifications to the 2MASS model calibration noted in the recent CRMBA paper. These very slightly affect the JHK_S model colors ($J \rightarrow J - 0.017$; $H \rightarrow H + 0.016$; $K_S \rightarrow K_S + 0.003$) and indeed these improve the fits to the data.

In the following analysis, we transform the latest Victoria isochrones (D. A. VandenBerg et al. 2010, in preparation) using the MARCS and CRMBA color–$T_{\rm eff}$ relations and test how well they are able to reproduce the observed VJK_S colors of field subdwarfs and our cluster photometry. Whenever possible, distances derived from *Hipparcos* parallaxes, along with the most up-to-date estimates of the cluster metallicities, have been assumed. However this study is much less concerned with the absolute fit of the isochrones to the observed CMDs than with the extent to which a consistent interpretation of the same cluster can be found on different color planes. Since any inaccuracies in distance moduli or [Fe/H] should be evident in all color planes, they should not effect our overall conclusions (though the possibility that chemical abundance anomalies may be present, and that they might affect the fluxes in some filter bandpasses more than others should be kept in mind). This does, of course, have the caveat that the observations must be free from systematic errors and that the extinction in all color bands is accurately determined.

As previously mentioned, this paper provides an extension of the $BV(RI)_C$ study by VCS10 to the near-IR. Consequently, we have tried to ensure that the analysis of the color transformations for a given cluster is consistent across optical and infrared colors by employing identical isochrones (i.e., for the same

Table 3
Fiducial Sequence for the Open Cluster NGC 6791 as Shown in Figure 3

V	$V-J$
19.817	2.062
19.659	2.001
19.515	1.944
19.363	1.889
19.215	1.840
19.067	1.787
18.924	1.738
18.771	1.692
18.633	1.656
18.486	1.625
18.331	1.595
18.172	1.567
18.011	1.548
17.845	1.529
17.676	1.528
17.516	1.548
17.388	1.588
17.357	1.639
17.367	1.699
17.411	1.762
17.437	1.831
17.476	1.897
17.485	1.953
17.459	2.011
17.376	2.043
17.263	2.058
17.109	2.071
16.959	2.091
16.809	2.114
16.659	2.130
16.509	2.152
16.359	2.164
16.209	2.186
16.059	2.211
15.909	2.236
15.759	2.264
15.609	2.299

Table 4
Fiducial Sequences for the Globular Cluster M 71 as Shown in Figure 4

V	$V-J$	$V-K_S$
19.505	1.805	2.408
19.338	1.757	2.338
19.168	1.712	2.273
18.991	1.670	2.214
18.807	1.635	2.163
18.622	1.604	2.138
18.429	1.576	2.099
18.232	1.555	2.068
18.029	1.542	2.051
17.824	1.542	2.040
17.634	1.563	2.110
17.500	1.611	2.199
17.445	1.673	2.278
17.439	1.745	2.353
17.441	1.814	2.424
17.396	1.882	2.492
17.267	1.931	2.564
17.084	1.959	2.606
16.885	1.977	2.631
16.688	1.989	2.649
16.485	2.021	2.667
16.268	2.035	2.687
16.060	2.070	2.709
15.854	2.080	2.734
15.627	2.120	2.766
15.426	2.152	2.798
15.217	2.177	2.835
14.986	2.209	2.880
14.736	2.247	2.935
14.538	2.274	2.974
14.356	2.306	3.020
14.177	2.342	3.071
13.993	2.381	3.129
13.818	2.422	3.187
13.646	2.465	3.250
13.459	2.516	3.324
13.305	2.562	3.390
13.139	2.648	3.481
12.906	2.733*	3.619*
12.693	2.833*	3.800*
12.523	2.962*	3.970*
12.347	3.137*	4.164*
12.212	3.300*	4.350*
12.116	3.469*	4.552*
12.035	3.717*	4.883*
11.997	4.109*	5.401*

Notes. Due to the sparseness of the RGB, those points with V <13 are marked by asterisks to indicate they have large uncertainties associated with them.

age and metallicity) and by adopting the same values of the reddening and distance modulus (in the case of clusters which are in common with VCS10: M 67, NGC 6791, NGC 1851, M 5, M 92). Additionally, the V-band photometry of the clusters presented in the following sections is from the same catalogues (Stetson 2000; Stetson 2005) that were used for the comparisons presented by VCS10.

The extinction coefficients adopted in this work are $E(V-J)/E(B-V) = 2.25$, $E(V-K_S)/E(B-V) = 2.76$ and $E(V-H)/E(B-V) = 2.55$ (McCall 2004).

3.1. M 67 ([Fe/H] ≈ 0.0)

M 67 is a particularly well studied, relatively nearby open cluster, with a metallicity that is very close to solar, according to the results of high-resolution spectroscopy (Tautvaišiene et al. 2000; Randich et al. 2006). See VCS10 for a summary of its basic properties, together with supporting references. Because of its proximity, 2MASS JHK_S observations of M 67 reach well below the MSTO; consequently, the CMDs shown in Figure 10 could be produced simply by combining M 67 data from 2MASS (Skrutskie et al. 2006) with the latest reduction of the V-band photometry discussed by Stetson (2005). The isochrone in this figure is that for an age of 3.7 Gyr from Michaud et al. (2004), and just as VCS10 found from their comparisons of the same isochrone with $BV(RI)_C$ photometry, both the MARCS and CRMBA transformations to the $V-J$ and $V-K_S$ color planes enable the models to match the observed photometry exceptionally well over the entire range of luminosity that has been plotted. Indeed, the differences between the two color–$T_{\rm eff}$ relations are barely discernible. (Only in the case of M 67 have we compared theory and observations on a $[(V-H)_0, M_V]$-diagram. Although the isochrone fits the data quite well, there is a slight, apparently nearly constant offset between the two, which may be due to a small error in our assumed value of $E(V-H)$ or in the zero point of the H magnitudes derived from the MARCS model atmospheres.)

Table 5
Fiducial Sequence for the Globular Cluster M 5 as Shown in Figure 6

V	$(V-J)$
21.95	2.01
21.84	1.96
21.60	1.84
21.37	1.74
21.16	1.65
20.95	1.56
20.75	1.50
20.55	1.43
20.36	1.36
20.16	1.30
19.96	1.26
19.75	1.21
19.53	1.17
19.31	1.12
19.07	1.08
18.83	1.05
18.59	1.03
18.34	1.05
18.14	1.09
18.00	1.15
17.92	1.25
17.89	1.28
17.87	1.33
17.84	1.37
17.80	1.39
17.74	1.42
17.54	1.46
17.32	1.47
17.08	1.48
16.83	1.50
16.57	1.51
16.33	1.54
16.05	1.57
15.81	1.60
15.55	1.63
15.27	1.67
15.04	1.70
14.80	1.74
14.57	1.79
14.35	1.84
14.14	1.89
13.91	1.95
13.71	2.00
13.49	2.06
13.29	2.12
13.09	2.18
12.86	2.27
12.68	2.36
12.50	2.47
12.31	2.59

Table 6
Fiducial Sequence for the Globular Cluster NGC 1851 as Shown in Figure 5

V	$V-K_S$
21.993	2.087
21.856	2.020
21.729	1.959
21.609	1.904
21.473	1.844
21.344	1.789
21.212	1.741
21.077	1.696
20.938	1.652
20.797	1.611
20.655	1.573
20.510	1.536
20.360	1.502
20.212	1.472
20.052	1.444
19.893	1.419
19.731	1.402
19.564	1.393
19.399	1.400
19.159	1.457
19.063	1.511
18.996	1.575
18.952	1.644
18.923	1.725
18.906	1.797
18.876	1.868
18.806	1.914
18.695	1.963
18.557	1.998
18.401	2.024
18.245	2.064
18.083	2.081
17.917	2.099
17.740	2.117
17.570	2.136
17.410	2.155
17.237	2.177
17.050	2.202
16.885	2.237
16.720	2.262
16.540	2.292
16.342	2.348
16.180	2.389
16.027	2.420
15.857	2.475
15.702	2.519
15.558	2.568
15.403	2.617
15.262	2.665
15.113	2.708
14.964	2.768
14.815	2.818

3.2. NGC 6791 ([Fe/H] ≈ +0.3)

Being the most metal rich cluster in our sample (and only open cluster for which we have collected JK_S observations), NGC 6791 provides an important test of the color–$T_{\rm eff}$ relations applicable to super-metal-rich stars. Here we have adopted the recent [Fe/H] estimate from Boesgaard et al. (2009). This is consistent with Brogaard et al. (2010) who derived [Fe/H] = 0.29 ± 0.03 (random) ± 0.07 (systematic) in their spectroscopic analysis. Anthony-Twarog et al. (2007) have noted that the Carraro et al. (2006) determination of [Fe/H] = +0.38 for NGC 6791 should be reduced to ∼ +0.28 (hence in very good agreement with the Brogaard et al. result) if those authors had adopted $E(B-V) = 0.15$ in their analysis, instead of 0.09.

Because of its large distance and low Galactic latitude, reddening estimates of NGC 6791 vary considerably in the literature. As discussed by Chaboyer et al. (1999), the derived reddenings for NGC 6791 span the range $0.09 \leqslant E(B-V) \leqslant 0.26$. Kuchinski et al. (1995) have used subdwarf-B stars to provide a tight constraint on the reddening, finding $E(B-V) = 0.17 \pm 0.01$. This agrees well with the Schlegel et al. (1998) estimate of $E(B-V) = 0.155$ mag, which is also

Table 7
Fiducial Sequences for the Globular Cluster M 13 as Shown in Figure 7

V	$V-J$	$V-K_S$
22.039	2.011	2.606
21.884	1.939	2.513
21.740	1.883	2.416
21.606	1.832	2.344
21.460	1.766	2.267
21.306	1.709	2.176
21.173	1.653	2.120
21.030	1.596	2.042
20.891	1.541	1.988
20.761	1.501	1.931
20.640	1.455	1.868
20.502	1.414	1.801
20.372	1.368	1.760
20.249	1.334	1.712
20.112	1.299	1.662
19.979	1.260	1.620
19.839	1.220	1.578
19.700	1.182	1.518
19.560	1.146	1.491
19.411	1.119	1.454
19.263	1.095	1.419
19.113	1.063	1.397
18.962	1.042	1.369
18.800	1.024	1.342
18.637	1.008	1.320
18.472	0.999	1.327
18.306	0.999	1.338
18.152	1.014	1.368
18.022	1.043	1.430
17.923	1.083*	1.506*
17.842	1.139*	1.556*
17.751	1.192*	1.632*
17.692	1.242*	1.684*
17.642	1.290*	1.734*
17.548	1.331*	1.782*
17.420	1.360*	1.814*
17.271	1.381*	1.844*
17.112	1.397	1.868
16.952	1.411	1.888
16.786	1.424	1.907
16.433	1.451	1.945
16.104	1.478	1.974
15.747	1.511	2.031
15.585	1.527	2.050
15.408	1.546	2.072
15.214	1.569	2.104
15.036	1.601	2.145
14.880	1.620	2.173
14.715	1.643	2.215
14.546	1.667	2.249
14.393	1.697	2.298
14.238	1.722	2.342
14.088	1.748	2.379
13.945	1.774	2.415
13.800	1.802	2.475
13.646	1.843	2.529
13.499	1.875	2.573
13.360	1.907	2.628
13.211	1.944	2.689
13.051	1.999	2.768
12.923	2.053	2.818
12.787	2.104	2.880
12.642	2.182	2.952
12.487	2.258	3.058

Table 7
(Continued)

V	$V-J$	$V-K_S$
12.289	2.373	3.223
12.152	2.474	3.352
12.005	2.612	3.547
11.895	2.729	3.741

Notes. Due to the lack of sufficient data at some magnitudes, isochrones were used to determine the fiducial points indicated by asterisks. Therefore these points have large uncertainties associated with them.

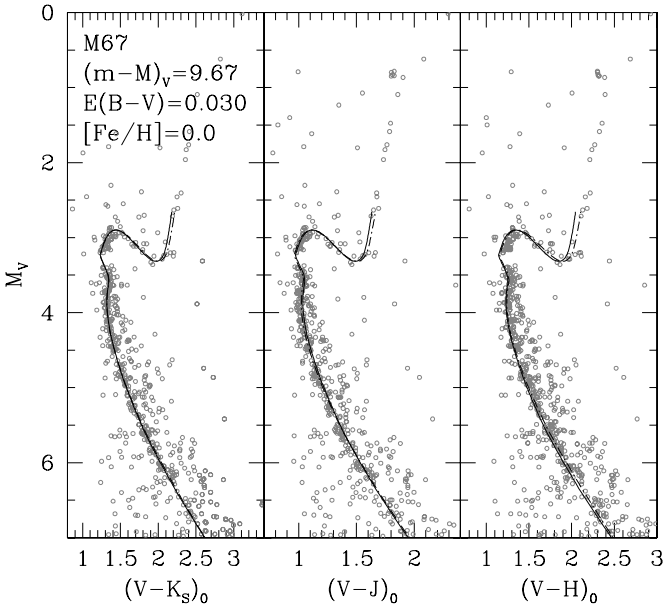

Figure 10. Comparison of a 3.7 Gyr isochrone for [Fe/H] = 0.0 with 2MASS/Stetson $V-K_S$, $V-J$, and $V-H$ observations of M 67. The solid and dot-dashed curves assume the MARCS and Casagrande et al. (2010) color transformations, respectively.

favored by the comparison of the NGC 6791 CMD with that for solar neighborhood stars from *Hipparcos* data (see Sandage et al. 2003). Additionally, Brogaard et al. (2010) also derived $E(B-V) = 0.160 \pm 0.025$, which adds to the support of our adopted reddening of 0.15.

In consistency with VCS10, we adopt a distance modulus of $(m-M)_V = 13.57$ which was found through a fit of the cluster CMD to local field dwarfs having metal abundances in the range $+0.15 \leqslant$ [Fe/H] $\leqslant +0.45$ and $\sigma(M_V) \leqslant 0.15$ (based on *Hipparcos* parallaxes). Figure 11 shows our $[(V-J)_0,\ M_V]$ CMD for dwarf and SGB stars in NGC 6791 is well reproduced by either the MARCS- or CRMBA-transformed Victoria isochrone on the assumption of the aforementioned reddening and distance. (Only along the upper RGB does the isochrone seem to deviate to the blue of the observations, which is consistent with the possibility that the MARCS atmospheres have insufficient blanketing in cool super-metal-rich stars.) Thus, there is excellent consistency with the isochrone fits reported by VCS10 to the $[(B-V)_0,\ M_V]$- and $[(V-I)_0,\ M_V]$-diagrams of NGC 6791. Since $E(V-J) = 2.25\ E(B-V)$ (e.g., McCall 2004), this consistency provides a further (strong) argument that the foreground reddening must, indeed, be quite close to $E(B-V) = 0.15$. This example thus provides an instructive example of how valuable it is to have both optical and near-

Table 8
Fiducial Sequences for the Globular Cluster M 92 as Shown in Figure 9

V	$V-J$	$V-K_S$
21.994	1.833	2.309
21.836	1.752	2.241
21.688	1.684	2.177
21.550	1.621	2.119
21.420	1.570	2.064
21.187	1.474	1.969
21.064	1.433	1.920
20.924	1.384	1.867
20.792	1.347	1.818
20.667	1.314	1.772
20.537	1.280	1.725
20.403	1.247	1.678
20.273	1.216	1.635
20.142	1.186	1.593
20.000	1.155	1.549
19.859	1.127	1.509
19.716	1.099	1.470
19.572	1.073	1.432
19.422	1.047	1.396
19.267	1.023	1.361
19.105	1.000	1.328
18.938	0.980	1.300
18.780	0.965	1.278
18.617	0.953	1.261
18.451	0.951	1.259
18.294	0.963	1.276
18.164	0.990*	1.314*
18.062	1.026*	1.365*
17.981	1.068*	1.415*
17.912	1.113*	1.450*
17.852	1.163*	1.521*
17.803	1.210*	1.589*
17.751	1.261*	1.662*
17.652	1.300*	1.723*
17.541	1.326*	1.758*
17.418	1.346*	1.800*
17.279	1.368*	1.832*
17.130	1.376*	1.857*
16.970	1.391*	1.880*
16.801	1.406*	1.901*
16.623	1.421*	1.922*
16.453	1.435*	1.942*
16.292	1.448	1.961
16.118	1.463	1.982
15.929	1.479	2.005
15.637	1.507	2.054
15.456	1.525	2.080
15.256	1.547	2.109
15.089	1.565	2.136
14.925	1.595	2.162
14.744	1.627	2.201
14.541	1.653	2.247
14.321	1.692	2.308
14.140	1.727	2.357
13.984	1.761	2.399
13.827	1.783	2.433
13.682	1.818	2.467
13.528	1.857	2.505
13.379	1.889	2.544
13.236	1.920	2.583
13.085	1.964	2.626
12.933	1.999	2.675
12.798	2.046	2.730
12.655	2.086	2.787

Table 8
(Continued)

V	$V-J$	$V-K_S$
12.503	2.147	2.854
12.362	2.208	2.922
12.235	2.262	2.998
12.103	2.332	3.108

Notes. Due to the lack of sufficient data at some magnitudes, isochrones were used to determine the fiducial points indicated by asterisks. Therefore these points have large uncertainties associated with them.

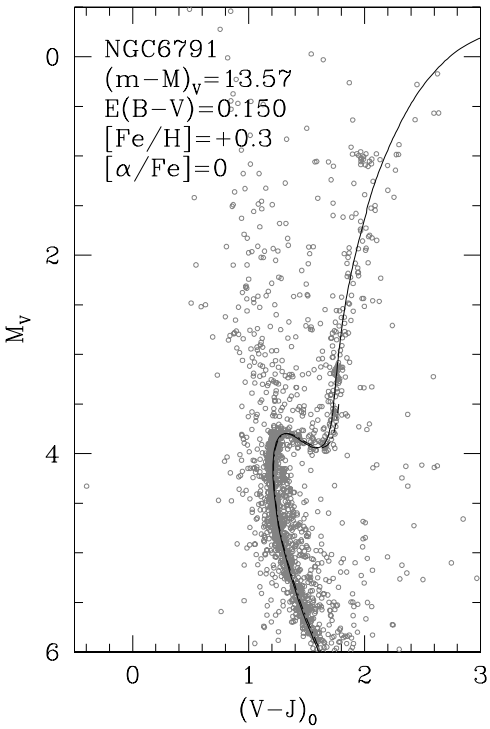

Figure 11. Comparison of an 8.0 Gyr isochrone for [Fe/H] = +0.3 and $Y = 0.30$ with our $V-J$ observations of NGC 6791. The solid and dot-dashed curves assume the MARCS and Casagrande et al. (2010) color transformations, respectively.

IR photometry to constrain the reddening in the case of highly reddened systems.

3.3. M 71 ([Fe/H] ≈ −0.75)

M 71 represents the metal-rich end of our sample of globular clusters (GCs). We adopt an [Fe/H] = −0.80 as derived by Boesgaard et al. (2005). It is quite obvious from the CMD in Figure 4 that this cluster has a low Galactic latitude, as contamination from field stars is still significant even when only those stars contained within an annulus of ∼7 arcmin around the cluster center are plotted. Furthermore, the Schlegel et al. (1998) dust maps indicate that the reddening is differential across the cluster, which contributes to the spread in color at any given magnitude, thereby hindering the definition of tight photometric sequences for this cluster in any photometric band.

As far as the cluster distance is concerned, we have adopted a distance modulus that leads to the most consistent interpretation between M 71 (in this paper), and that of 47 Tuc (in VCS10), which is known to have very close to the same metallicity. If the latter has $(m-M)_V = 13.40$, as assumed by VCS10, and if the

Table 9
Fiducial Sequences for the Globular Cluster M 15 as Shown in Figure 8

V	$V-J$	$V-K_S$
22.010	1.764	2.140
21.887	1.694	2.079
21.764	1.653	2.030
21.624	1.604	1.977
21.492	1.547	1.928
21.367	1.504	1.882
21.237	1.450	1.835
21.103	1.417	1.788
20.973	1.366	1.745
20.842	1.326	1.703
20.700	1.277	1.659
20.559	1.247	1.619
20.416	1.199	1.580
20.272	1.173	1.542
20.122	1.147	1.506
19.967	1.123	1.471
19.805	1.100	1.438
19.638	1.080	1.410
19.480	1.065	1.388
19.317	1.053	1.371
19.151	1.051	1.369
18.994	1.063	1.386
18.864	1.090	1.424
18.762	1.126	1.475
18.681	1.168*	1.535
18.612	1.213*	1.600
18.552	1.263*	1.671
18.503	1.310*	1.739
18.451	1.361*	1.772
18.352	1.400*	1.833
18.241	1.426*	1.858*
18.118	1.446*	1.900*
17.979	1.468*	1.932*
17.830	1.476*	1.957*
17.670	1.491*	1.980*
17.501	1.506*	2.001*
17.323	1.521	2.022
17.153	1.535	2.072
16.992	1.548	2.081
16.818	1.563	2.122
16.629	1.579	2.145
16.337	1.607	2.204
16.156	1.625	2.230
15.956	1.647	2.259
15.789	1.665	2.296
15.625	1.695	2.302
15.444	1.727	2.331
15.241	1.753	2.367
15.021	1.792	2.418
14.840	1.827	2.457
14.684	1.861	2.499
14.527	1.883	2.523
14.382	1.918	2.557
14.228	1.957	2.595
14.079	1.989	2.644
13.936	2.020	2.683
13.785	2.064	2.726
13.633	2.099	2.785
13.498	2.146	2.850
13.355	2.186	2.907
13.203	2.227	2.976
13.062	2.278	3.062
12.935	2.322	3.128
12.803	2.382	3.208

Notes. Due to the lack of sufficient data at some magnitudes, isochrones were used to determine the fiducial points indicated by asterisks. Therefore these points have large uncertainties associated with them.

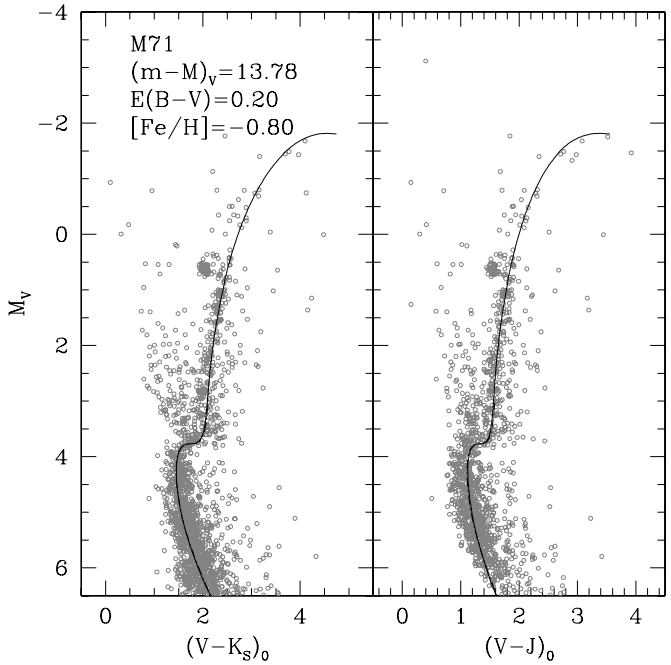

Figure 12. Comparison of an 11 Gyr isochrone for [Fe/H] = −0.75, with our observations of M 71. The solid and dot-dashed curves assume the MARCS and Casagrande et al. (2010) color transformations, respectively.

difference in magnitude of the HBs of 47 Tuc and M 71 is as given by Hodder et al. (1992), then a value of $(m-M)_V = 13.78$ is obtained for M 71.

Because of its low Galactic latitude ($b = -4.^\circ6$), M71 poses a challenge for reddening determinations: estimates in the literature range from $E(B-V) = 0.21$ to 0.32 (e.g. Kron & Guetter 1976; Harris 1996).

Figure 12 shows the isochrones compared with our observations. The observations are matched well by isochrones on the $[(V-K_S)_0,\ M_V]$-plane using either the MARCS or CRMBA color transformations. In the case of the $V-J$ observations, the isochrones match the base of the RGB well, but drift to the blue side of the lower MS, and to the red of the upper MS. However, the discrepancies at the faintest magnitudes may have an observational origin given that they arise close to the photometric limit of J. It should be noted that the reddening adopted here, $E(B-V) = 0.20$ was chosen to obtain a fit to the $B-V$ photometry. Thus, the models provide consistent interpretations across the $B-V$, $V-J$ and $V-K$ color planes.

3.4. M 5 and NGC 1851 ([Fe/H] ≈ −1.4)

As discussed quite extensively by VCS10, when Schlegel et al. (1998) reddenings are applied to the observed stars in M 5 and NGC 1851 and then their CMDs are shifted in the vertical direction so that the red HB populations of the two clusters have the same luminosities, one finds that the main-sequence fiducials of both clusters superimpose one another nearly perfectly, suggesting a common metallicity. This conflicts with the results of most spectroscopic studies, which indicate that NGC 1851 is ≈0.2 dex more metal rich than M 5 (e.g., Carretta et al. 2009; Kraft & Ivans (2003)). If this is correct, the latter should have a slightly brighter HB than the former, and therefore a slightly brighter MS at a given color—but this would be inconsistent with the assumed difference in [Fe/H] (unless Y or the heavy-element mixture also varies). However, a resolution of this issue is not important for the present investigation, which

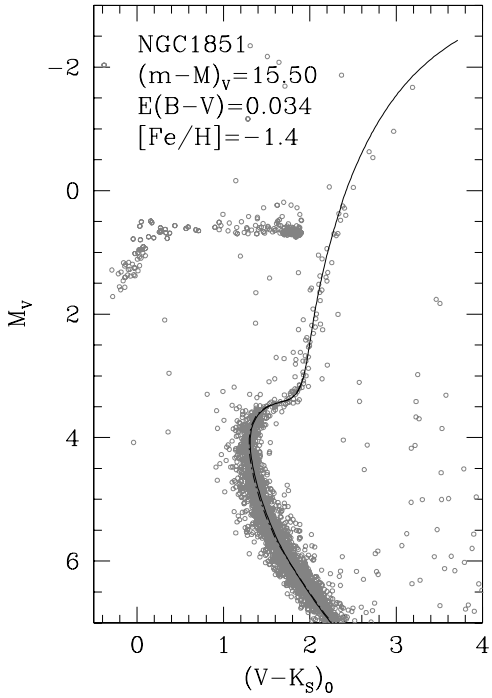

Figure 13. Comparison of an 11 Gyr isochrone for [Fe/H] = −1.4, [α/Fe] ≈ 0.4, and $Y = 0.25$ with our $V - K_S$ observations of NGC 1851. The solid and dot-dashed curves assume the MARCS and Casagrande et al. (2010) color transformations, respectively.

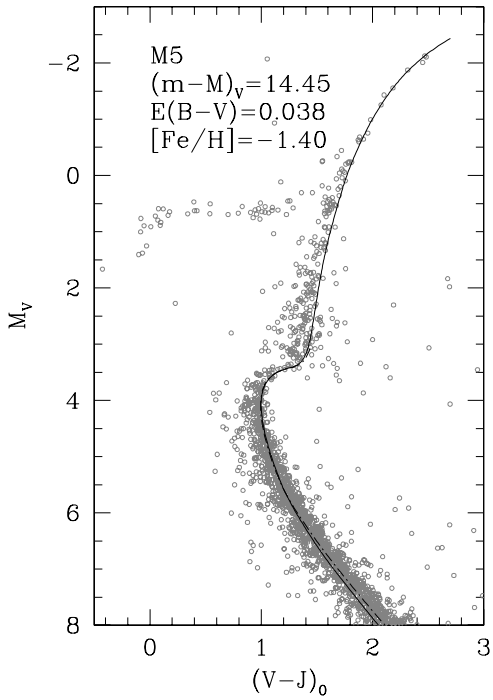

Figure 14. Same as the previous figure, except that the (same) isochrone is compared with our $V - J$ observations of M 5.

seeks to determine if consistent interpretations of the photometry across all color planes can be found. Following VCS10, we adopt [Fe/H] = 1.4 for both M 5 and NGC 1851 which is the metallicity which tends to be favored by stellar models such as VandenBerg (2000) (see VCS10 for a detailed description on this choice of metallicity).

In Figure 13, we overlay the same 11 Gyr isochrone used by VCS10 in their study of $BV(RI)_C$ photometry, onto the $[(V - K_S)_0,\ M_V]$-diagram of NGC 1851. For consistency with VCS10, we have adopted the same reddening and distance modulus; specifically, $E(B - V) = 0.034$ (Schlegel et al. 1998) and $(m - M)_V = 15.50$, based on observed and predicted HB luminosities (VandenBerg et al. 2000) as well as MS-fits of cluster fiducials to the CRMBA-transformed isochrones (and hence to the subdwarf standards for which these relations are defined; VCS10). We find that isochrones using the MARCS color–$T_{\rm eff}$ relations, or the CRMBA transformations for dwarf/SGB stars, are able to reproduce our $V - K_S$, V photometry of NGC 1851 rather well, except for the upper RGB (where there are few stars and where the stellar images are approaching the saturation limit). These results are fully consistent with those found by VCS10 when they analyzed $V - I$, V data. However, as they reported, the giant branch of the isochrone on the $[(B - V)_0,\ M_V]$-diagram is significantly bluer than the observed RGB. Thus, only the MS stars can be consistently fitted on all of the color planes that have been considered.

In the case of M 5, we have assumed that $E(B - V) = 0.038$ and $(m - M)_V = 14.45$ (see VCS10), which results in the comparison of the MARCS- and CRMBA-transformed isochrones with the $V - J$ observations shown in Figure 14. (Note that the isochrones are identical to those fitted to NGC 1851 photometry.) Given the differences in the relative positions of the RGBs of M 5 and NGC 1851 noted above, it is not surprising to find that, since the MARCS models are able to reproduce the giant branch of NGC 1851 in $V - K_S$ and $V - I$, they lie to the red of the observed RGB of M 5 in $V - J$ and $V - I$ (see VCS10, who also show that the predicted giant branch matches the $B - V$ colors of M 5 giants quite well). As far as the main sequence of M 5 on the $[(V - J)_0,\ M_V]$-diagram is concerned, the isochrones lie slightly blueward of the lower MS, and to the red of the upper MS, as seen in M71. As discussed below, this is also seen in the case of M 15 and M 92, and perhaps indicates that there is a small problem with the transformations to $V - J$.

3.5. M 13 ([Fe/H] ≈ −1.6)

For our comparisons with M 13, we have selected isochrones with [Fe/H] = −1.6 based on the work of Kraft & Ivans (2003). This is within 0.05 dex of the long favoured Zinn & West (1984) value of −1.65 and within 0.02 dex of the recent Carretta et al. (2009) value of −1.58. We have also adopted $(m - M)_V = 14.40$ which is very close to the value obtained by Grundahl et al. (1998) from a fit of Stromgren photometry to metal-poor subdwarfs with Hipparcos parallaxes, who also assumed [Fe/H] = −1.6. We adopt a reddening of $E(B - V) = 0.016$ from Schlegel et al. (1998). Additionally, Paltrinieri et al. (1998) derived δ(V) between M 3 and M 13 of 0.64 mag—so if M 3 has 15.00 (as adopted in VCS10), then 14.40 is implied for M 13 from the Paltrinieri et al result (if the 0.01 mag difference in reddening is taken into account).

In Figure 15, we compare a 12 Gyr isochrone with our VJ and VK_S photometry, finding that (for both colors) the isochrones provide a good match to the observed MS, but not to the observed RGB, which is significantly bluer at a fixed magnitude than the predicted colors. This is also found when fitting VI data (not shown here); i.e., when the same isochrones are overlaid onto $V - I$, V photometry, the main sequence is well matched but the predicted giant branch is offset to the red of the observed RGB. Interestingly, no such problem is found fitting the VI (or BV) photometry of M 3 (see VCS10), which is thought to have close to the same metal abundance as M 13.

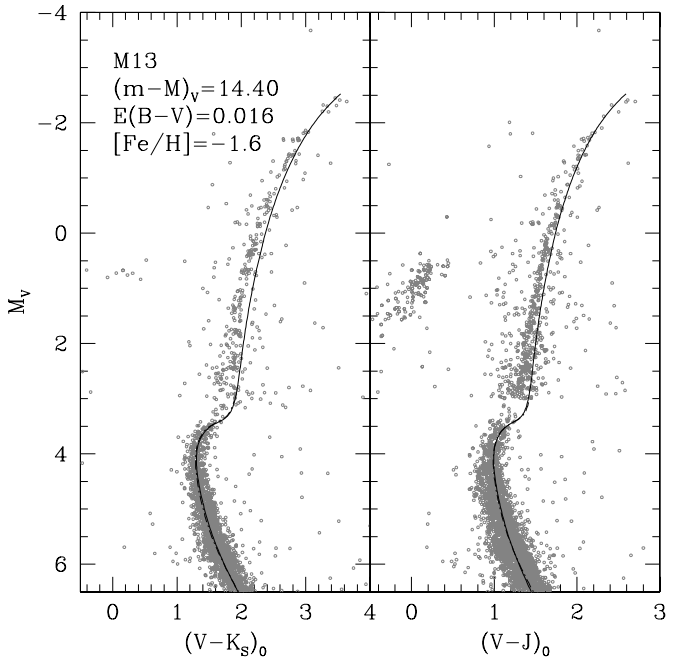

Figure 15. Comparison of a 12 Gyr isochrone for [Fe/H] = −1.60 with our observations of M 13. The solid and dot-dashed curves assume the MARCS and Casagrande et al. (2010) color transformations, respectively.

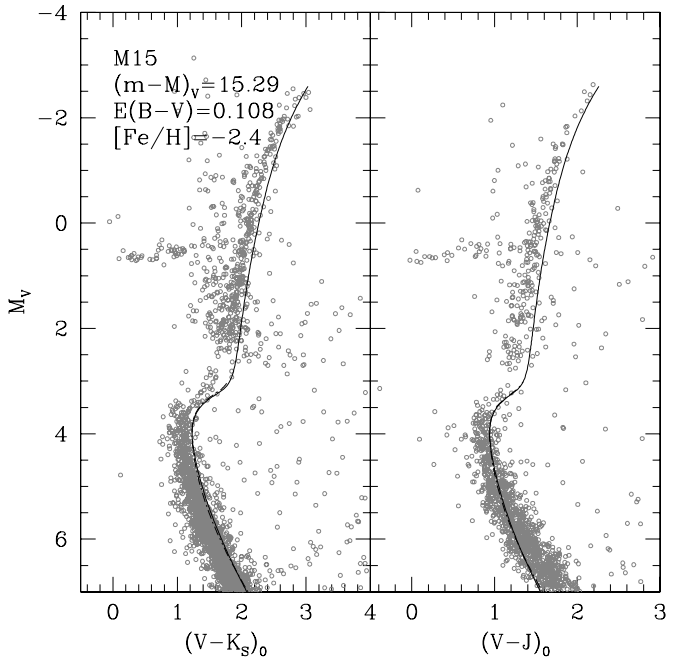

Figure 16. Comparison of a 13.5 Gyr isochrone for [Fe/H] = −2.40 with our observations of M 15. The solid and dot-dashed curves assume the MARCS and Casagrande et al. (2010) color transformations, respectively.

3.6. M 15 and M 92 ([Fe/H] ≈ −2.4)

M 15 and M 92 constitute the most metal poor clusters in our sample. For both clusters, a metallicity near [Fe/H] = −2.4 is consistent with the latest results from high-resolution spectroscopy (Kraft & Ivans 2003; Carretta et al. 2009). As regards their distances, we have adopted $(m - M)_V = 14.62$ for M 92 (see VandenBerg et al. (2002)), and $(m - M)_V = 15.29$ for M 15 given that Durrell & Harris (1993) have found that the main sequences of both clusters will superimpose one another if a vertical shift of 0.67 mag is applied to the M 92 CMD once their turnoff colors are matched. According to Schlegel et al. (1998), the reddenings of M 92 and M 15 are $E(B - V) = 0.023$ and 0.108 mag, respectively.

As shown by VCS10, a MARCS-transformed isochrone for 13.5 Gyr and [Fe/H] = −2.4 provides a reasonably good fit to both the BV and VI photometry of M 92—aside from the fact that a small color shift must be applied to the $V-I$ colors in order to obtain consistent fits to the various CMDs that can be generated from $BV(RI)_C$ photometry. Their additional observation that the isochrones tend to deviate to the blue side of the observed lower MS is apparently seen in especially the $[(V - J)_0, M_V]$-diagrams of M 15 and M 92 as well (see Figures 16 and 17). We have no explanation for such deviations, which appear to be most pronounced in the VJ photometry for M 15.

Perhaps the most serious concern is that, in both the $V-J$ and $V - K_S$ color planes, the isochrones lie consistently to the red of the observed RGBs of M 15 and M 92. Near the base of the giant branch, the offsets amount to ∼0.12 mag in $V - K_S$ and ∼0.09 mag in $V-J$ and the typical error in the photometry (∼0.02 mag) cannot explain these color offsets. Surprisingly, VCS10 find that the same isochrones provide a good fit to optical CMDs, apart from the small, constant offset between the predicted and observed RGB on the $[(V - I)_0, M_V]$-plane previously mentioned. Since we are using the same V-band photometry as VCS10, one might question the accuracy of the

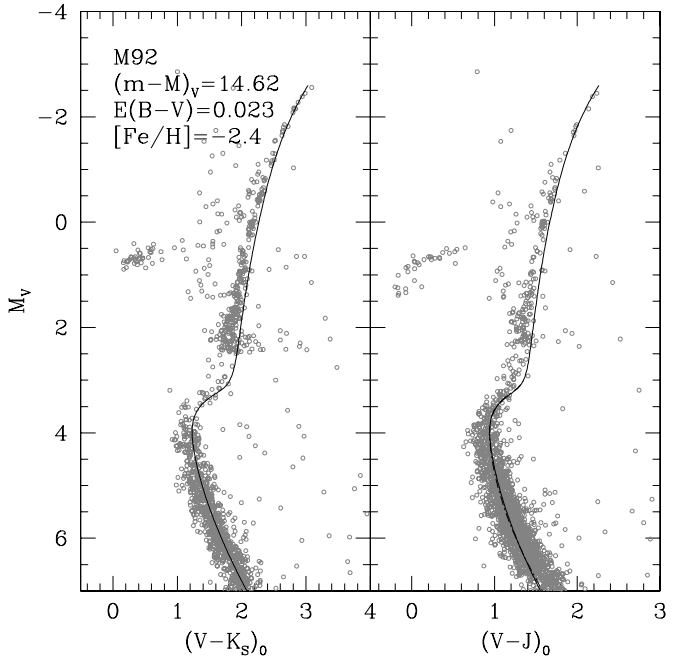

Figure 17. As in the previous figure, except that the (same) isochrone is compared with our observations of M 92.

J and K_S photometry for M 15 and M 92. However, this is not a viable explanation because the near-IR photometry for the cluster giants, as with all our CFHT clusters, comes directly from 2MASS, and such a large zero-point offset is highly unlikely. Indeed, because the isochrones reproduce $BV(RI)_C$ observations quite well, one wonders whether there is a problem with the synthetic J and K_S magnitudes that are derived from MARCS model atmospheres, though we have no other reason to question to these results. Further work is clearly needed to understand this puzzle.

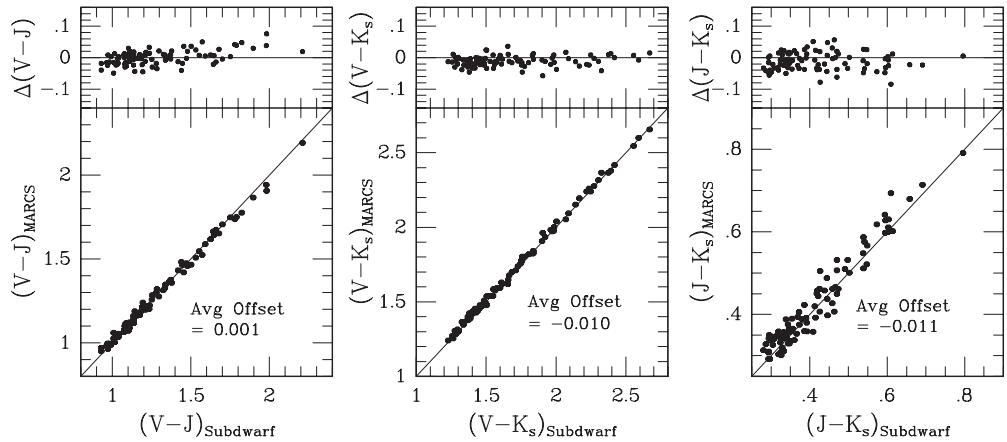

Figure 18. Comparison of the observed subdwarf colors with those predicted by MARCS color transformations on the assumption of the $T_{\rm eff}$, log g, and [Fe/H] determinations of CRMBA. The average offsets noted in each panel are relative to the observed colors. The upper panels plot the differences in the colors as a function of the subdwarf colors in the sense observed minus predicted.

3.7. Field Subdwarfs ($-2.2 \lesssim$ [Fe/H] $\lesssim -0.5$)

Subdwarfs are metal-poor stars with halo kinematics whose orbits have brought them into the solar neighborhood. With many of these stars having accurate distances determinations from *Hipparcos* and recent estimates of log g, and [Fe/H] based on high-resolution spectroscopy, they provide strong constraints on the $T_{\rm eff}$ scale of isochrones and color–$T_{\rm eff}$ relations at low metallicities. In the following analysis, we use a sample of ∼100 subdwarfs compiled by VCS10. The photometric and fundamental stellar properties (e.g., $T_{\rm eff}$, log g and [Fe/H]) for the majority of these stars were taken from Table 8 of CRMBA with the addition of four stars from Clementini et al. (1999). For a further description on the properties and choice of this sample, see VCS10.

In Figure 18 we show the level of agreement between the observed and predicted 2MASS colors, $(V - K_S)$, $(V-J)$, and $(J-K_S)$, of the subdwarfs in our sample. The predicted MARCS colors for each star are found by interpolating in tables of synthetic colors assuming the $T_{\rm eff}$, log g, and [Fe/H] values given by CRMBA. For these color–color comparisons we use only MARCS transformations since the CRMBA relations are themselves based on most of the same stars used here, so they will necessarily yield colors that agree well, in the mean, with the observed photometry. As noted in the three panels of Figure 18, offsets of ∼0.01 mag to the blue for the predicted $(V - K_S)$ and $(J - K_S)$ are needed to achieve consistency with observations. The predicted $(V-J)$ colors show a very small mean offset of 0.001 mag from the observed colors, though the largest deviations occur for the reddest stars, which suggests (perhaps) that the transformations to $V-J$ for cooler dwarf stars may need some adjustment. (Recall that, although this evidence is based on very few cool subdwarfs with measured $V-J$ colors, similar problems were seen in our comparisons with the $V-J$ photometry for MS stars in the low metallicity clusters M 92, M 15, M 13 and M 5; see the previous subsections.)

While the comparisons described above are completely independent of stellar evolutionary models, instructive comparisons of the theoretical isochrones with the *Hipparcos* subdwarfs can also be carried out. By superimposing subdwarfs onto a grid of isochrones for a wide range in [Fe/H] (and a fixed age—though isochrones exhibit essentially no age dependence at faint luminosities), it is possible to examine the consistency of the observed [Fe/H] values and colors with those inferred from the isochrones, given the observed temperatures. If a star lies on the same isochrone (say, one with [Fe/H] $= -1.5$) in all of the color planes, one can conclude that the color–$T_{\rm eff}$ transformations are consistent for those colors. If any obvious discrepancies exist for different filter combinations, then this is an indication of a problem with the color–temperature relations for one or more color indices (i.e., they do not adequately represent the spectrum of a star in the wavelength ranges spanned by the relevant filters).

In the lower panel of Figure 19, we superimpose *Hipparcos* (van Leeuwen 2007) subdwarfs onto 12 Gyr Victoria isochrones for [Fe/H] values from −2.4 to −0.6 (in the direction from left to right) transformed into the $[(V-J)\ M_V]$-, $[(V-K_S,\ M_V]$,- and $[(J-K_S),\ M_V]$-planes using the MARCS transformations. For each subdwarf, the CRMBA estimate of its [Fe/H] value minus the [Fe/H] value of the isochrone on which the subdwarf is located is plotted in the middle panel, while the upper panel plots the difference between the observed subdwarf color and that of the isochrone which has the same metallicity as the star (at the same M_V). These panels provide a measure of the quality of the fit to the observations. For example, if the isochrones were too red, most of the points would have positive δ[Fe/H] values and negative δ(color) values. Figures similar to 19 and 20, but for the $(B - V)$, $(V - R)$, and $(V - I)$ color planes, are given in the study by VCS10, where the individual subdwarfs are identified.

The subdwarfs in the $V - K_S$ and $V-J$ color planes show significant relative shifts with respect to the isochrones (i.e., the subdwarfs do not lie on the same position relative to the same isochrone in both colors). However, the scatter on the δ[Fe/H] and δ(color) planes is quite symmetric overall in both $V - K_S$ and $V-J$, with most of the redder stars having negative δ[Fe/H] and positive δ(color) values, whereas most of the bluer stars have positive δ[Fe/H] and negative δ(color) values. Thus, the isochrones are consistent with the observations, in the mean, with only a slight trend in the sense that the isochrones are somewhat too blue for the redder stars and too red for the bluer stars.

A different conclusion is drawn regarding the $J - K_S$ transformations shown in the right panel of Figure 19; the MARCS-transformed isochrones imply implausibly low values of [Fe/H], which are contrary to the implications from the other color planes. When looking at the δ[Fe/H] and δ(color) plots in the upper panels, one finds that most of the points have

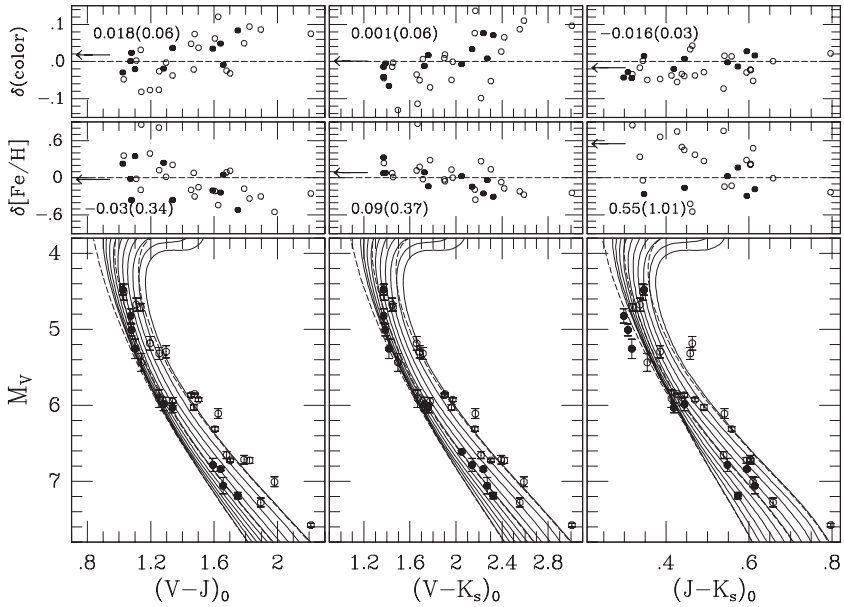

Figure 19. Lower panels: sample of *Hipparcos* subdwarfs overlying 12 Gyr Victoria isochrones in the $[(V-J)_0,\ M_V]$-, $[(V-K_S)_0,\ M_V]$- and $[(J-K_S)_0,\ M_V]$-planes. The isochrones plotted here have [Fe/H] values of −2.4 to −0.6 in increments of 0.2 dex, from left to right, and MARCS transformations have been used to transpose the models to the various CMDs. To demonstrate the age insensitivity for magnitudes $M_V \geqslant 4.5$, dashed lines show 10 Gyr isochrones for [Fe/H] = −0.6, −1.4, and −2.4. The photometry and metallicity of each subdwarf is taken from CRMBA, and the error bars represent 1σ uncertainties in the M_V values as derived from *Hipparcos* parallaxes. Subdwarfs having [Fe/H] $\leqslant -1.2$, as given by CRMBA, are plotted as filled circles, and those with higher metallicities are plotted as open circles. Middle panels: plotted as a function of color, the difference between the CRMBA estimate of [Fe/H] for each star and that inferred from the interpolated (or extrapolated when necessary) isochrone that matches its location on the color–M_V diagram in the lower panel. The arrows and the numbers, together with the standard deviation (in parentheses), indicate the mean δ[Fe/H] for all of the subdwarfs that have been considered. Upper panels: The difference in color that would need to be applied to each subdwarf in order to achieve perfect consistency of its position relative to the isochrones in the lower panel. n this case, the arrows and numbers indicate the mean values of δ(color) for the subdwarf sample.

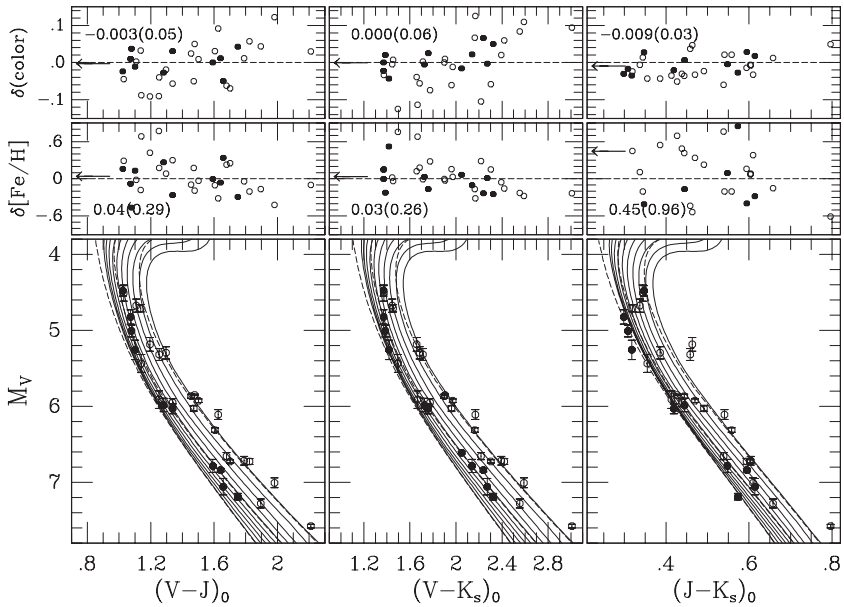

Figure 20. Similar to the previous figure, except that the isochrones are transformed using the color–$T_{\rm eff}$ relations developed by CRMBA.

positive δ[Fe/H] and negative δ(color) values, indicating that the isochrones are too red, in the mean, relative to the observations. The $J-K_S$ panels also indicate that there is no obvious trend with color or with metallicity.

Figure 20 plots the same isochrones as in Figure 19, but transformed to the various color planes using the CRMBA color–$T_{\rm eff}$ relations. When comparing the subdwarf colors and metallicities with those of the isochrones, we find there is no obvious trend with either color or metallicity, which indicates that the CRMBA-transformed isochrones agree well, in the mean, with the observations, while the absence of trends provides a verification that the functional form used in CRMBA transformations well represents the (bulk of) stars upon which it is built.

4. SUMMARY

We have derived fiducial sequences for the Galactic star clusters M 15, M 92, M 13, M 5, NGC 1851, M 71, and NGC 6791 (encompassing $-2.4 \lesssim$ [Fe/H] $\lesssim +0.3$) using near-IR

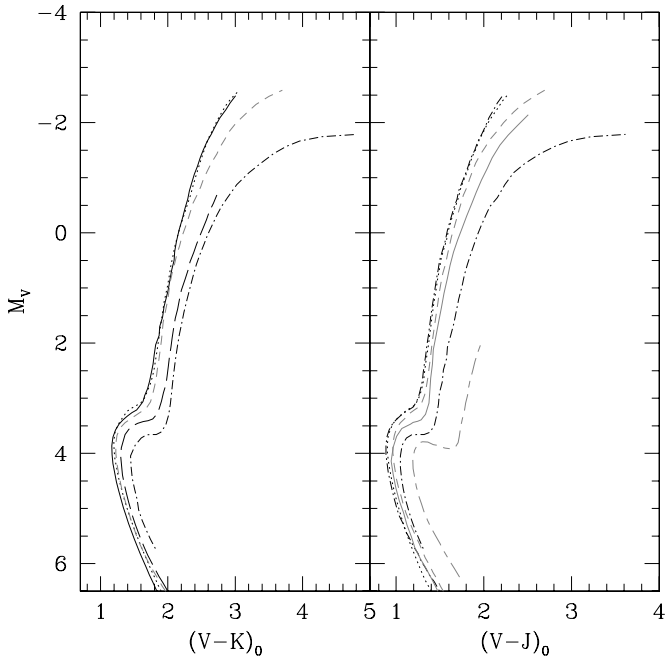

Figure 21. Our cluster fiducials mapped to the $[(V-K_S)_0,\ M_V]$- and $[(V-J)_0,\ M_V]$-planes using the reddenings and distance moduli given in Table 2. From left to right, corresponding to increasing metallicity, are M 15 (solid black), M 92 (dotted black), M 13 (gray short-dashed), NGC 1851 (black long-dashed), M 5 (black solid line), M 71 (black dot-dashed), and NGC 6791 (gray long-short dashed).

observations obtained with the WIRCam imager on the CFHT and the HAWK-I detector on the VLT. These fiducial sequences, which are presented in Figure 21 on the $[(V-J)_0,\ M_V]$- and $[(V-K_S)_0,\ M_V]$-planes, illustrate how the photometric properties of these old stellar populations vary as a function of [Fe/H]. With spectroscopic metallicity determinations and relative age estimates that are accurate to within ± 0.25 dex and ± 1.5–2 Gyr, respectively, these fiducials can, in principle, be used to photometrically determine the age and metallicity of resolved stellar systems. Unlike isochrone analyses, metallicity determinations made through comparisons with fiducials are independent of stellar evolutionary models. Hence, these fiducials provide a set of empirical isochrones that can serve as valuable tools for future stellar population investigations involving the 2MASS filters.

Based on these data, a summary of our results is as follows.

1. The predicted $V-J$, $V-K_S$, and $J-K_S$ colors given by the MARCS transformations for local subdwarfs agree well with those observed (i.e., to within $\sim$0.01 mag) when the temperatures and metallicities of the latter are as given by CRMBA.
2. While isochrones appear to be too blue when compared with lower main sequence stars in metal-poor GCs on the $[(V-J)_0,\ M_V]$-plane, no significant problems are found matching their $V-K_S$ colors.
3. Our analysis of cluster RGB stars indicates that the isochrones and the color transformations faithfully reproduce the properties of metal-rich giants, but not those of lower metallicity. In fact, the RGB segments of the isochrones become systematically redder than the observed RGBs with decreasing [Fe/H]. It seems unlikely that errors in the model $T_{\rm eff}$ scale are sufficient to cause this problem, because the discrepancies are primarily on the $V-J$ and $V-K_S$ color planes. The same MARCS-transformed isochrones are able to reproduce the CMDs of M 92 derived from $BV(RI)_C$ photometry quite well. This seems to suggest that there are problems with the predicted J and K_S magnitudes at low metallicities, but we are not able to provide an explanation for the origin of such difficulties.

This work has been supported by the Natural Sciences and Engineering Research Council of Canada through a Discovery Grant to D.A.V. We are grateful to the anonymous referee for valuable comments. Additionally, C.M.B. thanks Loic Albert and Aaron Dotter for insightful discussions which improved both the observations and analysis in this paper.

REFERENCES

Anthony-Twarog, B. J., Twarog, B. A., & Mayer, L. 2007, AJ, 133, 1585
Boesgaard, A. M., Jensen, E. E. C., & Deliyannis, C. P. 2009, AJ, 137, 4949
Boesgaard, A. M., King, J. R., Cody, A. M., Stephens, A., & Deliyannis, C. P. 2005, ApJ, 629, 832
Brogaard, K., Bruntt, H., Grundahl, F., Clausen, J. V., Frandsen, S., VandenBerg, D. A., & Bedin, L. R. 2010, A&A, in press (arXiv:1009.5537)
Carraro, G., Villanova, S., Demarque, P., McSwain, M. V., Piotto, G., & Bedin, L. R. 2006, ApJ, 643, 1151
Carretta, E., Bragaglia, A., Gratton, R. G., D'Orazi, V., & Lucatello, S. 2009, A&A, 508, 695
Casagrande, L., Portinari, L., & Flynn, C. 2006, MNRAS, 373, 13
Casagrande, L., Ramírez, I., Meléndez, J., Bessell, M., & Asplund, M. 2010, A&A, 512, 54 (CRMBA)
Chaboyer, B., Green, E. M., & Liebert, J. 1999, AJ, 117, 1360
Clem, J. L., Vandenberg, D. A., Grundahl, F., & Bell, R. A. 2004, AJ, 127, 1227
Clementini, G., Gratton, R. G., Carretta, E., & Sneden, C. 1999, MNRAS, 302, 22
Durrell, P. R., & Harris, W. E. 1993, AJ, 105, 1420
Ferraro, F. R., Montegriffo, P. A., & Fusi-Pecci, F. 2000, AJ, 119, 1282
Frogel, J. A., Persson, S. E., & Cohen, J. G. 1983, ApJ, 53, 713
Grocholski, & Sarajedini., 2003, MNRAS, 345, 1015
Grundahl, F., VandenBerg, D. A., & Andersen, M. I. 1998, ApJ, 500, 179
Gustafsson, B., Edvardsson, B., Eriksson, K., Jorgensen, U. G., Nordlund, A., & Plez, B. 2008, A&A, 486, 951
Harris, W. E. 1996, AJ, 112, 1487
Hodder, P. J. C., Nemec, J. M., Richer, H. B., & Fahlman, G. G. 1992, AJ, 103, 460
Kraft, R. P., & Ivans, I. I. 2003, PASP, 115, 143
Kron, G. E., & Guetter, H. H. 1976, AJ, 81, 817
Kaluzny, J., & Rucinski, S. M. 1995, A&AS, 114, 1
Kuchinski, L. E., Frogel, J. A., Terndrup, D. M., & Persson, S. E. 1995, AJ, 109, 1131
McCall, M. L. 2004, AJ, 128, 2144
Michaud, G., Richard, O., Richer, J., & VandenBerg, D. A. 2004, ApJ, 606, 452
Paltrinieri, B., Ferraro, F. R., Fusi Pecci, F., & Carretta, E. 1998, MNRAS, 293, 434
Pinsonneault, et al. 2004, ApJ, 600, 946
Randich, S., Sestito, P., Primas, F., Pallavicini, R., & Pasquini, L. 2006, A&A, 450, 557
Sandage, A. R., Lubin, L. M., & VandenBerg, D. A. 2003, PASP, 115, 1187
Schlegel, D. J., Finkbeiner, D. P., & Davis, M. 1998, ApJ, 500, 525
Skrutskie, M. F., et al. 2006, AJ, 131, 1163
Stetson, P. B. 1987, PASP, 99, 191
Stetson, P. B. 2000, PASP, 112, 925
Stetson, P. B. 2005, PASP, 117, 563
Stetson, P. B., & Harris, W. E. 1988, AJ, 96, 909
Tautvaišiene, G., Edvardsson, E., Tuominen, I., & Ilyin, L. 2000, A&A, 360, 495
Valenti, E., Ferraro, F., & Origlia, L. 2007, AJ, 133, 1287
VandenBerg, D. A. 2000, ApJS, 129, 315
VandenBerg, D. A., Casagrande, L., & Stetson, P. B. 2010, AJ, 140, 1020 (VCS10)
VandenBerg, D. A., & Clem, J. L. 2003, AJ, 126, 778
VandenBerg, D. A., Richard, O., Michaud, G., & Richer, J. 2002, ApJ, 571, 487
VandenBerg, D. A., Swenson, F. J., Rogers, F. J., Iglesias, C. A., & Alexander, D. R. 2000, ApJ, 532, 430
van Leeuwen, F. 2007, A&A, 474, 653
Zinn, R., & West, M. J. 1984, ApJS, 55, 45